CONF-8406137--4

SELF-BREAKDOWN SPARK GAP STABILITY UNDER REP-RATE CONDITIONS*

L. F. Rinehart and M. T. Buttram
Sandia National Laboratories
Albuquerque, NM 87185

Abstract

We have measured the statistical distribution of self-breakdown voltages of a spark gap at very low repetition rates (< 1 Hz) and at 20 and 40 pulses per second. For the high repetition rate experiments, the test switch discharged a resistively charged energy storage capacitor into a resistive load producing a simple R-C relaxation waveform across the spark gap. Typical discharge parameters were in the 10 to 35 kV, 10 to 20 kA range with about 1 μs pulse width. For the low rate work, a 20% reversal ringing waveform was used to reach higher discharge currents (up to 100 kA). An on-line computer data acquisition system was used to record and process large numbers of breakdowns, thus producing good statistical samples.

The data show two distinct instabilities. At high currents (> 30 kA) those data that have a single simple distribution are of an extreme value form that is skewed toward low voltage. At low currents and higher repetition rates, the data evolve from a narrow DC (single pulse) breakdown voltage distribution into a broader Gaussian distribution at 20 pulses per second (pps) and finally to a very broad bimodal distribution (two Gaussians) at 40 pps. At 40 pps some firings occur as low as 30% of the mean. Effects of pressure and flow rate on the distributions are presented, and we discuss possible explanations for the origins of the distributions and their behavior.

Introduction

Spark gap breakdown can be an unstable process, particularly when high currents and repetition rates are involved. Under such conditions, breakdown voltage stability can become very poor, with erratic low voltage firings, "dropouts," occurring a substantial fraction of the time at voltages below 50% of the mean self-break level.

Most pulsed power machines use triggered gas dielectric spark gaps, at least in the initial stages of power compression. It is desirable to operate these gaps near their self-breakdown level to reduce jitter and the required triggering energy. However, because of the erratic low voltage breakdowns which occur in rep-rated gaps, the gaps would either have to be operated at a small fraction of self-break voltage or an intolerable pre-fire rate would result. The typical solution, purging the switch with many volumes of gas between shots, adds greatly to the overall system cost and complexity. With this dilemma in mind, we are trying to understand the origin of low voltage breakdowns in spark gaps and learn to reduce or eliminate them.

Experimental Apparatus and Method

A simple R-C relaxation oscillator, shown in the schematic in Fig. 1, was used for the high repetition rate tests. The energy storage capacitor C was charged through R_C and discharged, via the gap, into R_L. We designed the apparatus to generate at maximum 850 J, 0.025 C pulses at a 100 Hz repetition rate with a charging voltage of 70 kV. For the low rate, high current experiments, the spark gap charge was bipolar and the circuit impedance was more inductive than the high rep rate circuit. Figure 1 also shows the general physical layout of the apparatus. Both R_C and R_L were flowing water resistors with a flow rate of a few tens of gallons per minute. The charging resistor was a parallel plate type filled with deionized water. Its resistance was 10 to 50 kΩ, typically. The water lines leading to R_C have a resistance to ground 1800 times greater than R_C, and this effect on the circuit performance was negligible. A coaxial geometry was used for R_L, which helped to keep the series inductance of the circuit low. The value of the resistor was selected so that the circuit was critically damped or just underdamped. Laundry soap[1] was added to the resistor's water to lower ρ and obtain the desired resistance. The soap solution is less reactive with the metallic parts of the resistor and the pump than the more commonly used $CuSO_4$. The water pipes were connected to the resistor's outer grounded conductor; therefore, they did not contribute to the circuit.

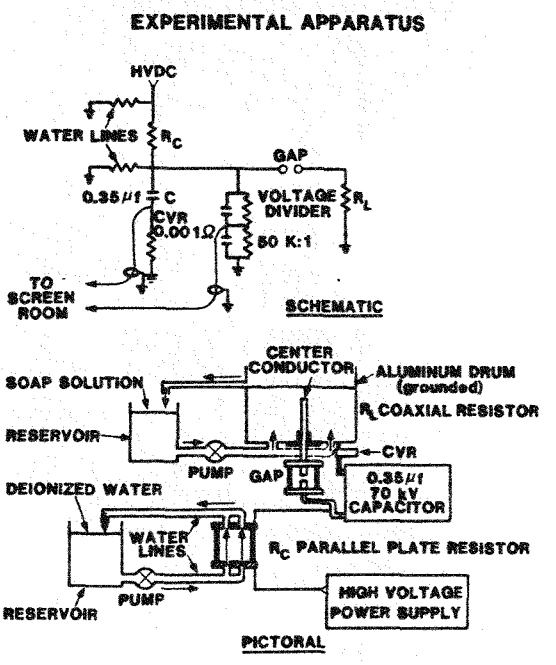

Figure 1. Schematic and pictoral diagrams of the experimental apparatus.

Water for both R_C and R_L circulated through the resistors from two reservoirs, the thermal mass of which absorbed the energy dissipated in the resistors. In the case of R_L, during a typical run the water temperature in the reservoir increased from 20°C to 65°C and, as a consequence, ρ dropped to ≈ 1/2 its initial value. Decreasing ρ correspondingly decreases the value of the resistor. Allowing for the distributed inductance in the circuit, I_{peak} could increase by as much as 30% during a run.

*This work was supported by the U. S. Department of Energy under contract DE AC04-76-DP00789.

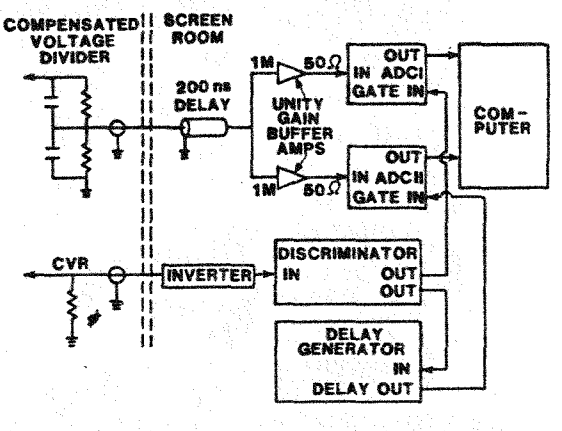

Figure 2. Schematic diagram of the data acquisition system.

Figure 2 is a schematic of the data acquisition system. For the sake of simplicity some pulse shaping gates and attenuators have been omitted from the drawing. A compensated resistor-capacitor voltage divider was used to monitor the voltage across the energy storage capacitor. A 0.001 Ω CVR (current viewing resistor) was used to monitor the current. Signals from the two probes were brought into the screen room on equal-length coaxial cables. When a discharge occurred, the CVR signal triggered a discriminator circuit that generated two simultaneous output pulses. One output gated the analog to digital converter (ADC I), which read the voltage into the computer. There was a 200 ns delay line between the voltage divider and ADC I; therefore, when ADC I was gated it read the voltage 200 ns before the discharge occurred. Reading the voltage just before the breakdown did not result in an error, because in the dV/dt range of the R-C circuit there was virtually no voltage rise in 200 ns. We ensured that a false trigger would not send incorrect data to the computer by using the second output of the discriminator, delayed several microseconds, to gate ADC II: If a discharge had occurred, the output of ADC II would be near zero because the energy storage capacitor could not recharge significantly in that time. If ADC II read significant voltage into the computer, the computer disregarded the entire event.

The computer was programmed to calculate the mean value, standard deviation, and repetition rate of the incoming data. When a run was terminated, the computer generated a histogram of the data it had received between manually initiated start and stop points. By manually starting and stopping the data flow to the computer, the effects of raising and lowering the power supply voltage and any "first pulse" or conditioning effects could be edited out of the final data. A large number of measurements are required to provide a good statistical sample; typically, 10^4 to 10^5 breakdowns were measured during each run.

We used a spark gap of ACF-10-Q POCO[2] graphite electrodes with approximately uniform field geometry. The electrode spacing was 0.635 cm and the diameter was 5.1 cm with a 0.95 cm exhaust hole in the center. The overall surface of the electrodes was flat and the outer edge and exhaust hole of each electrode had a 0.64 and 0.32 cm radius respectively. Gas flowed radially into the gap volume and out the central (axial) exhaust hole of each electrode. Unless otherwise stated, air was the dielectric gas.

We measured the gap's breakdown voltage at DC (single pulse) and at 20 and 40 pps at various pressures. We were able to hold the rep rate steady to within ∓ 5% in most cases. The DC measurements were made with no gas flow and the 20 and 40 pps measurements at various flow rates. When we specify flow rates in terms of volumes/shot we mean the "active" 5.1 cm diameter x 0.635 cm (19.4 cm^3) cylindrical gap volume rather than the volume of the entire gap housing.

Experimental Results

Low current DC (< 30 kA) breakdowns were generated by raising the gap voltage < 1 kV/second. We tested the gap at pressures from 1 to 2.5 atmospheres and in every case DC breakdowns occurred in a very narrow distribution, all within ∓ 0.6% of the mean.

At rep rates of 20 pps and below, we observed that breakdown voltage (V_B) had a normal (Gaussian) distribution but with much more scatter than the DC breakdown. The 20 pps data are shown in a cumulative probability graph in Fig. 3. Plotted is the cumulative probability of breakdown (horizontal axis) as a function of voltage (vertical axis). The probability axis is so scaled that a straight line on this plot indicates a Gaussian distribution.[3] When the data are a single Gaussian, its peak is at the voltage corresponding to a 50% cumulative probability (50 on the horizontal axis). The slope of the line is a measure of the width of the Gaussian. The standard deviation is one-half the voltage interval between the 16% and 84% points on the probability axis. Note that the distributions in Fig. 3 are Gaussian with about the same standard deviation (σ) regardless of pressure or flow rate (within the limits of the experiment) over a range of probability from <1% to >99%. Breakdown occurs increasingly farther below the DC breakdown level as pressure is increased. The important point is that increasing the repetition rate from single pulse to 20 pps increases the distribution width by a large factor, typically ± 10 to 15% of the mean, but does not skew the distribution toward low voltage.

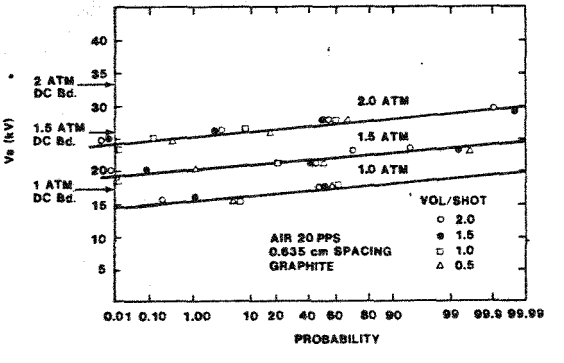

Figure 3. Normal cumulative probability plot of 20 pps data at various pressures and flow rates.

As the rep rate of the switch is further increased, a "tail" begins to grow on the low voltage side of the distribution. This negative skew is shown in a typical histogram of 40 pps data in Fig. 4.

Qualitatively, this histogram appears to contain the Gaussian from the 20 pps data plus an additional distribution at lower voltage.

Figure 5 shows the cumulative probability versus breakdown voltage for 1, 1.5, 2, and 2.5 atmosphere pressures at 40 pps. The S-shaped tails appearing on the left ends of these otherwise normal distributions indicate the mixing in of another lower voltage distribution in varying proportions.(3)

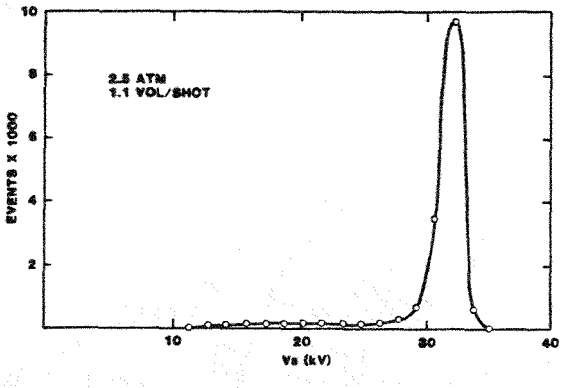

Figure 4. Histogram of 40 pps data at 2.5 Atm pressure 1.1 volume/shot flow.

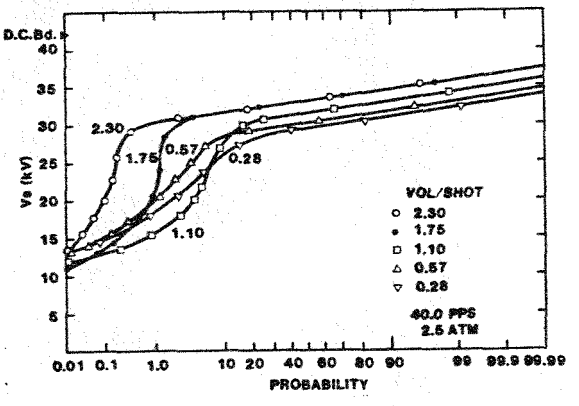

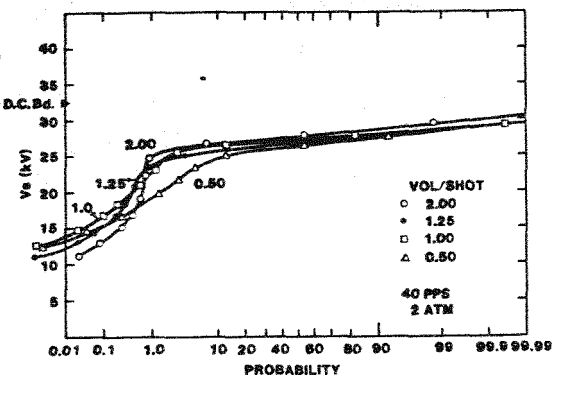

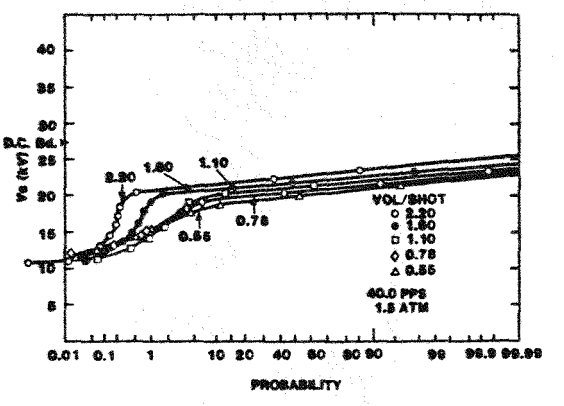

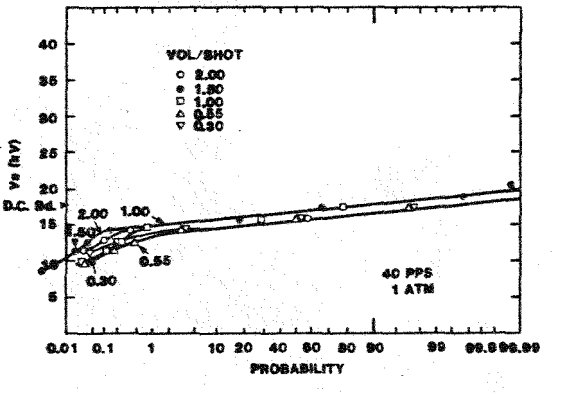

Figure 5. Normal cumulative probability plots of 40 pps data at various pressures and flow rates.

Using standard interpretation methods, we estimate the relative proportions of the mixed distributions from the inflection points of the S curves. The cumulative probability of the component distributions is then calculated, treating all data points above and below the inflection point of the original curve as two separate distributions.(4) Some small uncertainty remains concerning the data points near the inflection point, but this method provides adequate resolution for our purposes. For purposes of discussion, we call the lower distribution $\Delta\ell$ and the higher Δh.

The resolved component distributions are shown in Fig. 6 for 1.5, 2, and 2.5 atmosphere pressures. The 1 atm data are obviously bimodal also, but there are not enough data points in $\Delta\ell$ to resolve it. Examining the component distributions reveals that the higher components are similar to the corresponding 20 pps distributions except for a slight tendency for σ to increase with pressure. Note also that $\Delta\ell$ and Δh tend to diverge (the peak of $\Delta\ell$ moves down and Δh moves up) as flow is increased. This is shown graphically in Fig. 7. These histograms present only the lower few percent of the data on an expanded scale (as compared to Fig. 4). At 2.5 atmospheres, the distributions are thoroughly mixed at 0.5 volume/shot; somewhat more separate at 1 volume/shot; and totally separate at 2.3 volume/shot. With a few exceptions, σ is independent of flow in both $\Delta\ell$ and Δh. In $\Delta\ell$, there is a noticeable trend for σ to increase with pressure.

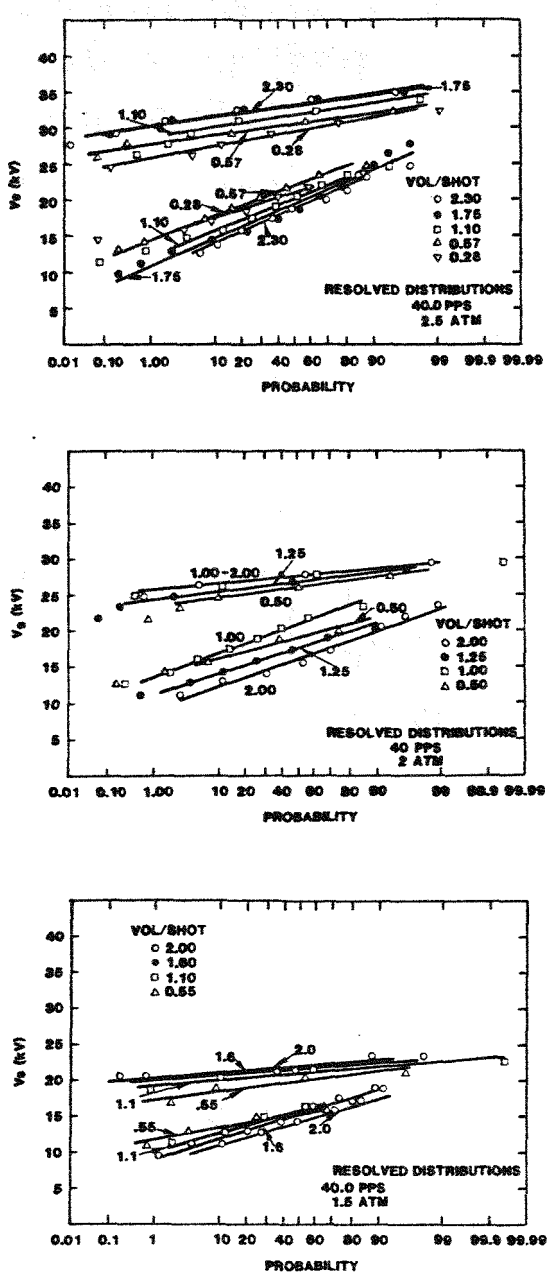

Figure 6. Normal cumulative probability plots of resolved component distributions from 40 pps data at various pressures and flow rates.

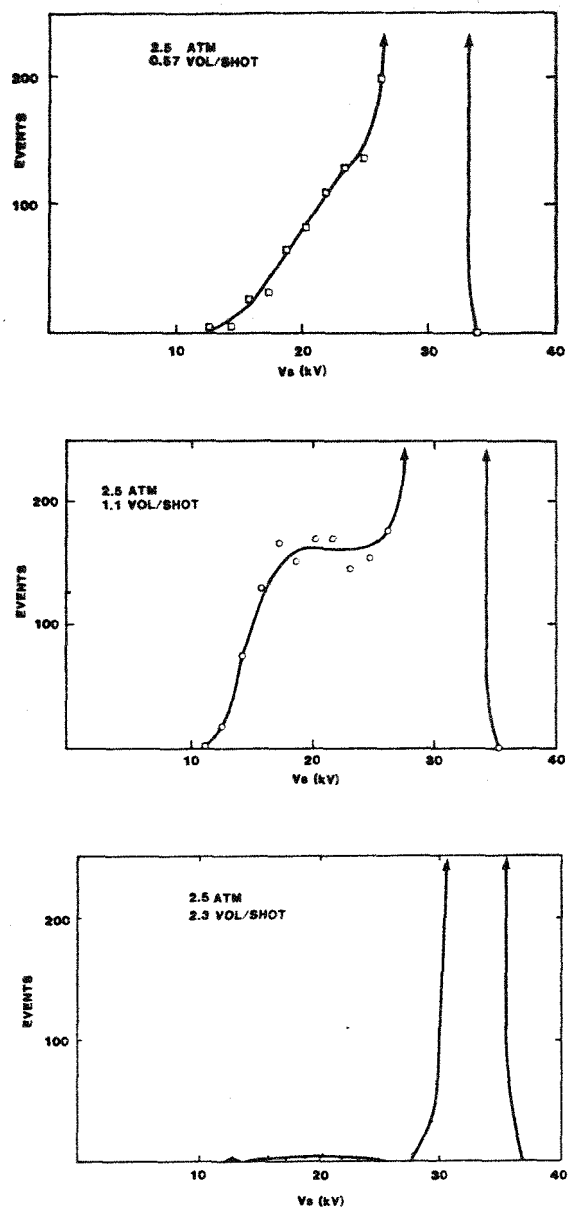

Figure 7. Histograms showing effect of flow rate on $\Delta\ell$ in the 40 pps data.

We found that both pressure and flow influence the relative proportions of $\Delta\ell$ and Δh. The percentage of the total population of events which occurs in $\Delta\ell$ is plotted in Fig. 8 as a function of flow at each pressure. There is considerable overlap and scatter in the data due to statistics and limitations on the size of the histogram bins. Nevertheless, the data show a definite tendency for the percentage of the total population which falls into $\Delta\ell$ to increase with pressure and, especially at higher pressures, to decrease with flow. As previously mentioned, both components of the bimodal distributions tend to hold their standard deviations constant with respect to flow rate, but σ increases with pressure; the lower distribution much more strongly than the higher. Figure 9 illustrates this observation and also shows the 20 pps data for comparison. It is clear that the 40 pps Δh and the 20 pps data have essentially the same standard deviation. From line Δh in Fig. 10, it is also clear that their peaks follow the same straight line as a function of pressure. Clearly, they can be assumed to arise from the same process whereas the $\Delta\ell$ distribution at 40 pps apparently arises from a different mechanism.

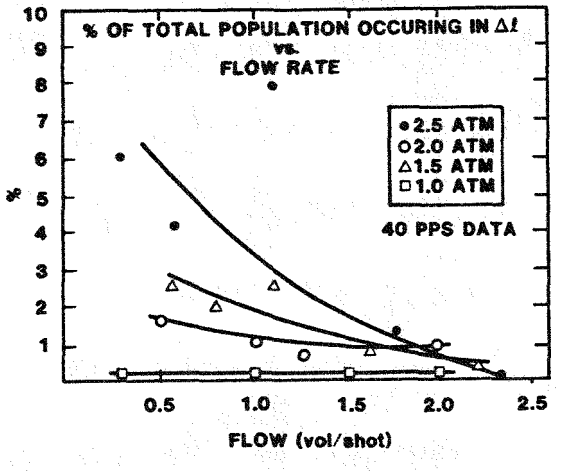

Figure 8. Effects of pressure and flow rate on the relative proportions of $\Delta\ell$ and Δh.

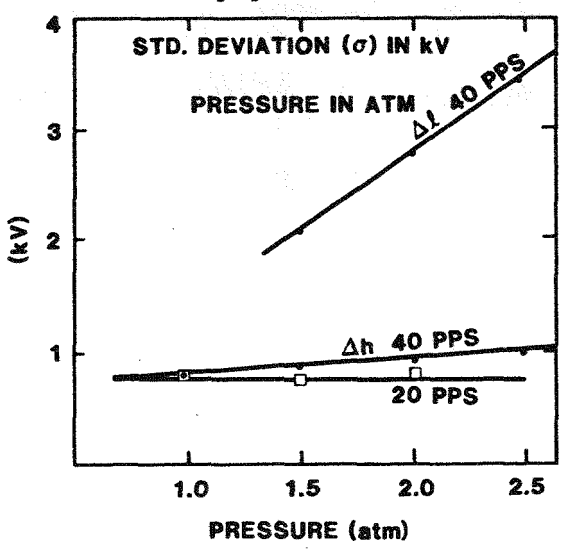

Figure 9. Comparison of standard deviation of 20 pps data with $\Delta\ell$ and Δh from 40 pps data.

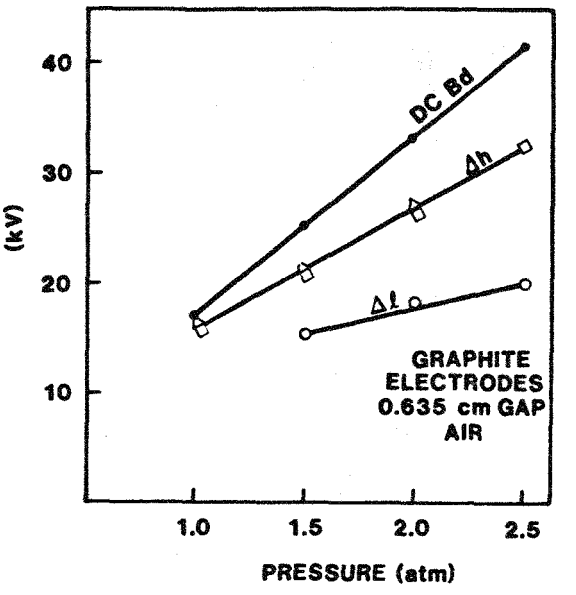

△ AVE OF ALL FLOW RATES @ 20 PPS

□ AVE OF ALL FLOW RATES @ 40 PPS Δh MEAN VALUES

○ AVE OF ALL FLOW RATES @ 40 PPS Δℓ MEAN VALUES

Figure 10. Breakdown voltage as a function of pressure for DC, 20 pps and the component distributions at 40 pps.

Turning to the higher current low repetition rate data, we see another distinguishable form of low voltage instability. Figure 11 is an illustrative differential probability histogram for sulfur hexafluoride gas and brass electrodes. The discharged current at the peak of the voltage distribution is 90 kA. The data were taken at 0.13 pps average. There is a pronounced peak and a low voltage tail extending to 65% of the peak. This is typical of the extent of the tail at the 0.1% level.

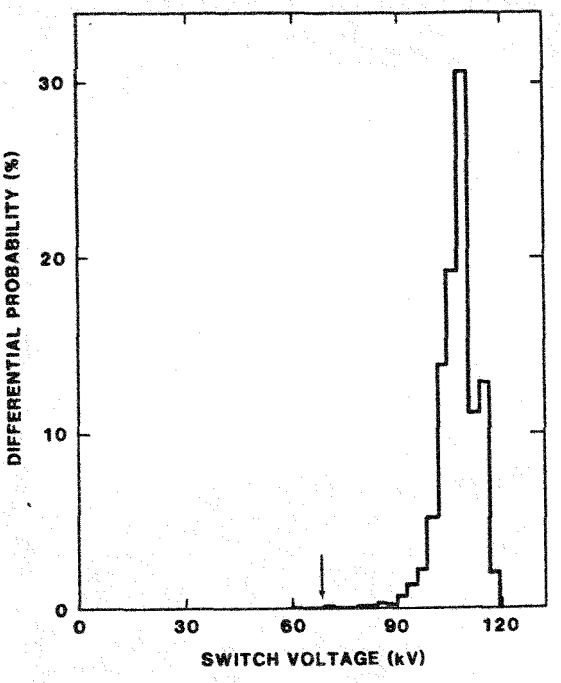

Figure 11. Differential probability histogram of high current 0.13 pps data with brass electrodes and SF_6 gas.

Additional data of this type were taken for brass electrodes in air and sulfur hexafluoride and for graphite electrodes in air. Figures 12-14 present, as a function of pressure, the peak of the voltage distribution with one standard deviation "error bars" together with the minimum (and in two cases the maximum) of the breakdown voltage distribution. The common trends are: (1) the peak voltage is linear in pressure, and (2) the minimum voltage drops away with increasing pressure following more closely a square root of pressure line in the case of the large statistical sample brass and air data. The current pulse (kA) following switch closure peaks at 80% of the voltage in kilovolts. From earlier data we know that the voltage dropouts do not occur if a 5 kΩ resistor is placed in the discharge circuit. It is reasonable then to assume that the dropouts result from the high current. The dropouts have largely disappeared when the current (voltage) is below 25 kA (30 kV). This is consistent with the earlier repetitive data which showed no dropouts at or below 20 Hz at 10 to 20 kA.

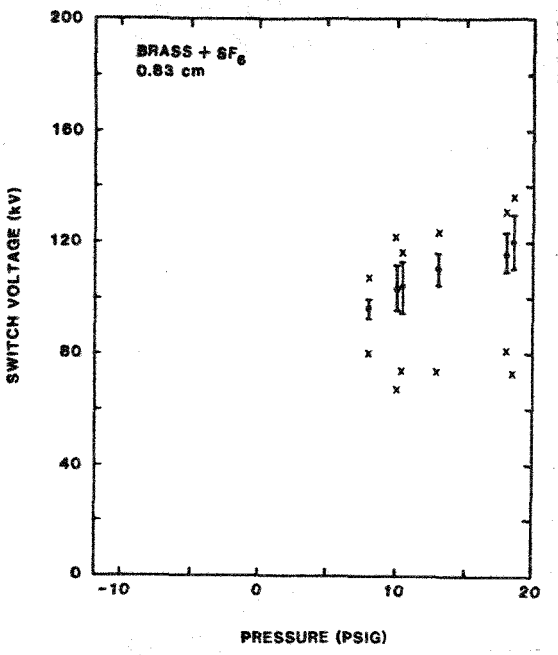

Figure 12. Peaks of voltage distribution ± σ and high and low points as a function of pressure with high current discharge.

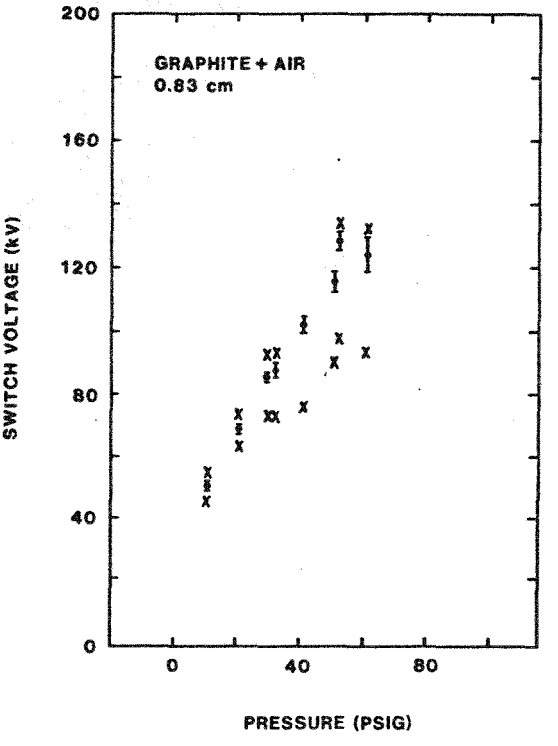

Figure 13. Peaks of voltage distribution ± σ and high and low points as a function of pressure with high current discharge.

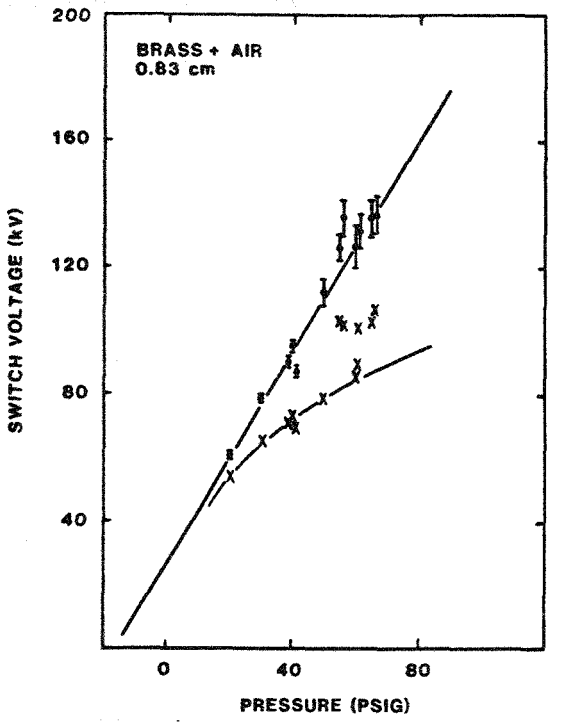

Figure 14. Peaks of voltage distributions ± σ and low points as a function of pressure with high current discharge.

The data, when they are distributed according to a single distribution, follow the extreme value distribution. Figure 15 presents the data from Fig. 11 on an extreme value plot, i.e., a plot analogous to the Gaussian plots used earlier where now the extreme value distribution follows a straight line. The extreme value distribution is characteristic of weak link failure. Extreme value distributions have been observed to characterize the tensile strength of materials and the failure of capacitors. It is not surprising, therefore, to find it in gas breakdown. The data clearly show that it is generated by high currents not by high repetition rates.

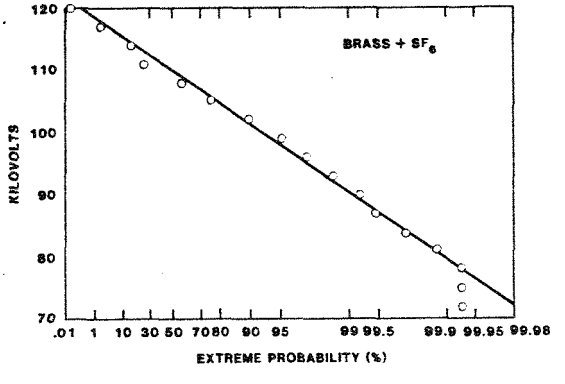

Figure 15. Extreme value cumulative probability plot of high current 0.13 pps data with brass electrodes and SF_6 gas (from Fig. 11).

Discussion

Other experimenters have observed bimodal distributions in electrical breakdowns. Feser[5] found two mixed Gaussian modes in lightning waveform data with long rod-rod and rod-plane gaps. He found the higher voltage distribution to be associated with streamer corona and the lower distribution with leader corona. Gray and Harrington[6] have shown bimodal distributions in some close spaced surface flashover experiments. Nitta et al.[7] observed that a normal breakdown distribution in SF_6 transitions to an extreme value distribution as pressure, area, or volume effects begin to dominate the breakdown conditions. This is consistent with the idea that low voltage breakdowns are a result of low probability surface defects. Larger areas have a higher probability of having a fatal defect. High pressures aggravate the effect of a given defect. This situation has been analyzed for microprotrusions by Avrutskii.[8] Our data linking the extreme value instability to the current that causes the surface damage completes this picture.

In Fig. 10, the 20 pps data and the component distributions of the 40 pps data are compared to the DC breakdown level as a function of pressure. The fact that all the rep-rate data fall below the DC breakdown level might be explained by heating of the dielectric gas. At our maximum flow rate of 2 vol/shot at 40 pps, the mean radial gas velocity in the gap volume is 203 cm/sec. The molecular speed in air (at 0° C and 1 Atm) is > 48×10^3 cm/sec; therefore, hot gas will diffuse out of the gap volume against even the strongest flow. After a few moments of running the switch at some rep rate and flow, the entire gas volume of the switch housing should come to thermal equilibrium at a temperature somewhat above ambient. We do, in fact, notice that when a rep-rate run is started the breakdown voltage creeps down (and consequently the rate rises) for the first few moments. We edit this effect out of our data by the method described earlier. The gas temperature rise T_R necessary to cause a given drop in the peak V_s of the upper breakdown voltage distribution can be estimated. For a first order approximation, we assume the breakdown voltage is a linear function of gas density. At a given pressure, density will vary according to the relation $P = nkT$. It follows that the temperature necessary to reduce the voltage by the observed amounts is $T = T_o\ (V_o/V_{rep})$ and the expression for the temperature rise is then $T_R = 300°K\ [(V_o/V_{rep})-1)]$. The following table gives V_s at DC and 40 pps and T_R at each pressure. The 40 pps breakdown voltages are the average of the mean values of the resolved higher distributions at all flow rates. The 20 pps data follow closely, as was seen in Fig. 10.

Table I: Gas Temperature Rises

Pressure (Atm)	V_s DC (kV)	V_s 40 pps (kV)	T_r (°C)
1	17.4	16.7	13
1.5	25.8	21.1	67
2	32.9	27.5	59
2.5	41.3	31.7	91

The temperature calculation is very sensitive to small voltage changes so the error in T_R may be large. Nevertheless, these temperatures are reasonable considering that the gas is recovering from an arc temperature of several thousand degrees and the variation of the upper Gaussian's parameters are

consistent with thermal effects. Parker, et at,[9] have shown that beyond 4 ms, the electrode tips tend to be hotter than the dielectric gas. Thus, these temperature rises most likely occur in the boundary layer gas. The electrodes could be heated by ion bombardment, which would give a heating rate proportional to the gap current (voltage) or by Joule heating (current or voltage squared). Our data are unable to discriminate between these two. The lower distribution probably is not a simple heating effect because its peak shifts to lower voltage with increased cooling flow. Nevertheless, it is a rate dependent phenomenon appearing when the interpulse period becomes shorter than the accepted 90 to 100% recovery time of unpurged spark gaps (5 to 50 ms). It becomes increasingly important at higher pressures like the tail of the high current (extreme value) distribution but is a distinct phenomenon, being a Gaussian. At this point its origin remains uncertain.

A probable effect of the lower Gaussian can be seen in previously published spark gap data. Table II lists the parameters of four air spark gaps described in the literature. Generally it was necessary to extrapolate the data actually reported to derive a volumes per shot number.

Table II: Spark Gap Purging Characteristics

Voltage	Rep. Rate	Volumes/Shot	Ref.
25 kV	20 to 40	8 - 15	10
100 kV	250	4	11
50 kV	1000	5 - 8	12
130 kV	40	4 - 16	13

Repetition rate varies over a factor of 50, voltage over a factor of 5, and the gas flow geometry is either rotary (vortex)[10,12,13] or axial.[11] The switches were run for at least 1000 shots continuously with these parameters and were triggered.

Interestingly, all the authors found that 4 to 8 volume exchanges were necessary in reasonable agreement with Fig. 8 which shows that something in excess of two volumes per shot are needed to suppress $\Delta\ell$. It is reasonable to suppose then that for this variety of repetitive spark gaps, the purpose of gas flow is to suppress the lower Gaussian distribution. From these results plus preliminary data from our experiment using other gases and electrode materials, one can infer that the occurrence of the lower Gaussian is more general than our graphite-air example and one may speculate that its parameters may not change grossly with gap construction or materials.

Conclusions

In summary, we find that at least two processes cause erratic low voltage firings: (1) Damage to the electrode surfaces caused by high current. This process is characterized by the extreme value distribution. (2) High rep-rate effects, which generate a separate and distinct low voltage distribution. This distribution mixes in varying proportions with the otherwise acceptable Gaussian high voltage breakdown distribution.

We find that below the threshold of electrode damage (≈ 30 kA), single pulse breakdowns have a very narrow distribution where all firings occur within ± 0.6% of the mean. At low rep rates (20 pps), the narrow single pulse distribution evolves into a lower voltage, broader Gaussian where all breakdowns typically occur within ± 10 to 15% of the mean. The rep-rate mean breakdown voltage is reduced from DC level by an amount consistent with residual thermal effects. Finally, when the rep rate is increased from 20 to 40 pps, we observe a very broad bimodal distribution in which both components are Gaussian. The higher voltage component is essentially identical to the low rep rate distribution and can be assumed to arise from the same mechanism. The low voltage component behaves differently and must be assumed to originate from a different process. The low voltage distribution can be manipulated by varying pressure and flow rate. Its origin remains unclear.

We are designing additional experiments which should yield further information on rep-rate switch stability. Higher rep rates, higher voltage and current, and other conditions which should extend the present trends and introduce electrode effects are planned.

References

1. Private conversation with Dr. G. M. Molen, Old Dominion University, Norfolk, VA.

2. Poco Graphite, Inc.
1601 Smith State Street
Decatur, TX 76234

3. J. R. King, Probability Charts for Decision Making (New York, Industrial Press Inc. 1971) p. 23-39.

4. S. Peck, Accelerated Testing Handbook (Technology Associates, Portola Valley, CA, 1978) p. 3-8/3-10.

5. K. Feser, Proc. IEE, 1309-1313 (1971).

6. E. W. Gray and D. J. Harrington, JAP 53, 237 (1982).

7. T. Nitta, N. Yamada, and Y. Fujivara, Proc. IEEE Power Engineering Society, 623 (1973).

8. V. A. Avrutskii, G. M. Goncharenko, and E. N. Prokhorov, Sov. Phys. Tech. Phys., Vol. 18, No. 3, p. 386-388, Sept. 1973.

9. A. B. Parker, D. E. Poole, and J. F. Perkins, Brit. J.A.P., Vol. 16, p. 851-855, 1965.

10. G. J. Rohwein, Proc. 1980 14th Power Modulator Symposium, Orlando, FL, p. 1.

11. A. Ramrus, IEEE Trans on Electric Development Vol. ED-26, NO. 10, Oct. 1979.

12. J. T. Naff, et al, 1980 14th Power Modulator Symposium, Orlando, FL, p. 21.

13. R. Limpaecher and R. Schneider, Proc. 1982 15th Power Modulator Symposium, Baltimore, MD, p. 75.